Available online at www.sciencedirect.com
SCIENCE DIRECT®
Journal of Sound and Vibration 290 (2006) 169–191
JOURNAL OF SOUND AND VIBRATION
www.elsevier.com/locate/jsvi

Complete balancing of a disk mounted on a vertical cantilever shaft using a two ball automatic balancer

C. Rajalingham, R.B. Bhat*

Department of Mechanical and Industrial Engineering, Concordia University, Montreal, Quebec, Canada

Received 6 October 2004; received in revised form 7 March 2005; accepted 21 March 2005
Available online 12 July 2005

Abstract

An automatic balancer is a simple device consisting of several balancing balls, which are guided to move in a circular track. The suitability of a two-ball automatic balancer to balance the residual unbalance in a vertical rotor is investigated. The combined dynamical system consisting of the rotor and the balancer has a balanced steady state together with a set of unbalanced steady states. Under certain conditions, the balls ultimately position themselves so as to balance the system completely. A linearized analysis is initially used to have an insight into the stability of the balanced steady state of the system. Subsequent nonlinear response analysis showed that the scope of the linear analysis is severely limited to predict the stability of balanced steady state. The nonlinear analysis revealed that, under certain conditions, the system ultimately settles down to the balanced steady state and thereby balance the residual unbalance in a vertical rotor completely.

1. Introduction

In high-speed machinery applications, the imbalance in the rotor introduces an unwanted dynamic load, which causes the rotor shaft to whirl about its axis [1,2]. This imbalance can be minimized by balancing the rotor as far as possible. In an experimental study, Lindell used an automatic balancing device to reduce the unbalance vibration in a hand-held grinding machine [3].

*Corresponding author. Tel.: +1 514 848 3109; fax: +1 514 848 4509.
E-mail address: rbhat@vax2.concordia.ca (R.B. Bhat).

0022-460X/$ - see front matter © 2005 Elsevier Ltd. All rights reserved.
doi:10.1016/j.jsv.2005.03.025

Nomenclature

$(a_{Cx'}, a_{Cy'})$	acceleration components of point C
c_B	damping coefficient for balancing ball motion in track
$\bar{c}_B$	$\bar{c}_B = c_B/m_B\omega_0$
c_R	damping coefficient for rotation of disk
$\bar{c}_R$	$\bar{c}_R = c_R/I\omega_0$
c_T	damping coefficient for translation of disk
$\bar{c}_T$	$\bar{c}_T = c_T/m\omega_0$
EI	flexural rigidity of shaft
$\mathbf{F}_{ED}$	force at C due to elasticity
$\mathbf{F}_{IB}$	force due to inertia of balancing ball
$\mathbf{F}_{ID}$	force due to inertia of disk
$(\mathbf{i}, \mathbf{j}, \mathbf{k})$	unit vectors for $Oxyz$ frame
$(\mathbf{i}', \mathbf{j}', \mathbf{k}')$	unit vectors for $Cx'y'z'$ frame
I	rotor inertia about transverse axis
$\bar{I}$	$\bar{I} = I/ml^2$
k_0	$k_0 = 3EI/l^3$
l	length of cantilever shaft
m	mass of disk
m_B	mass of balancing ball
n	number of balancing balls
$\mathbf{M}_{ED}$	moment at C due to elasticity
$\mathbf{M}_{ID}$	moment at C due to inertia of disk
p	frequencies of linearized system
p_0	forward frequencies of rotor
q_0	forward frequencies of rotor in stationary frame
R	radius of track on disk
s	complex frequency
$(v_{Cx'}, v_{Cy'})$	velocity components of point C
(x_C, y_C)	coordinates of mounting point C
$(\bar{x}_C, \bar{y}_C)$	$\bar{x}_C = x_C/\delta$, $\bar{y}_C = y_C/\delta$
(α, β, γ)	rotations of shaft at C
$(\bar{\alpha}, \bar{\beta})$	$\bar{\alpha} = \alpha l/\delta$, $\bar{\beta} = \beta l/\delta$
δ	unbalance eccentricity
λ	$\lambda = m_B R/m\delta$
Λ	$\Lambda = \delta/R$
μ	$\mu = 4/3\bar{I}$
ν	$\nu = m_B/m$
ω	angular velocity of rotor
ω_0	$\omega_0 = \sqrt{k_0/m}$
$(\omega_{x'}, \omega_{y'}, \omega_{z'})$	angular velocity components of disk
Ω	$\Omega = \omega/\omega_0$
ψ_i	angular position of ith balancing ball
ψ_{10}, ψ_{20}	balanced positions of the balls

The balancing device was located on the grinder, which was mounted on a vertical shaft. In this device, several balancing balls were guided to move in an oil-filled circular track in a plane perpendicular to the rotor shaft. Additional information on the design and installation of the device is available in this reference. Under certain conditions, the balancing balls moved automatically to their steady-state positions and thereby reduced the rotor vibration due to unbalance whirling. In certain other circumstances, the performance of the automatic balancer was found to be unsatisfactory.

The stability of the dynamic system consisting of the rotor and the balancing device was considered to provide an insight into the effectiveness of the balancing device in rotor-dynamic applications. Rajalingham, Bhat and Rakheja studied the stability analysis of undamped dynamic system consisting of the Jeffcott rotor and a single-ball balancer [4,5]. This study utilized the linearized equations of motion to identify the stable speed range of the system. It indicated that the presence of the balancing ball can reduce rotor vibration in certain super-critical speed range of the system.

Hwang and Chung investigated the stability analysis in the application of a double race automatic balancing device to balance the Jeffcott rotor [6]. Linear viscous damping was included in the rotor-dynamic model and the linearized equations of motion were used for the stability analysis. They identified the balanced steady-state configuration and investigated the system stability of this balanced steady state using linearized equations of motion. Subsequently, Chung

and Jang extended the analysis for a cantilever rotor, by including the gyroscopic influence on the stability of the balanced steady-state configuration of the dynamic system [7].

In addition to the system damping, the nonlinearity of the governing equations has to be considered for realistic dynamic analysis of the system. Since the motion of the balancing ball in its track is not restrained, the angular positions of the balancing balls need not vary within small intervals. Consequently, the linearized equations cannot represent the dynamical system reasonably well. However, the stability analysis using the linearized equations can provide useful insight into the stability of the system. Finally, for accurate analysis of the system, the nonlinear equations must be used with an arbitrary set of initial conditions.

2. Theory

For the analysis, the rotor is modeled as a thin unbalance disk, which is mounted on a flexible, mass-less cantilever shaft at C, as shown in Fig. 1. As the shaft rotates, the disk undergoes translation and rotation in three dimensions. The displacement of the mounting point C in the longitudinal direction is second order compared to those in the transverse directions. A brief description of the kinematics that will be helpful in developing the equations of motion of the dynamical system consisting of the unbalanced disk and the balancer balls is presented below.

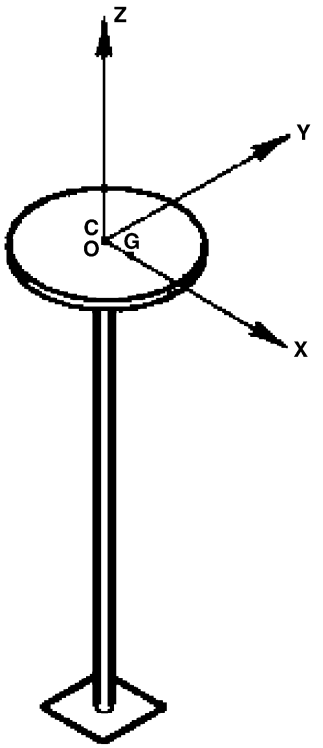

Fig. 1. Stationary frame $OXYZ$.

2.1. Kinematics of disk

Under certain conditions, the residual imbalance in the disk can be balanced by using an automatic balancing device. The device consists of a number of balancing balls that are guided to move in a circular track with center at C. A rotating reference frame, which is fixed on the disk at C, is used to express the equations of motion of this dynamic system. Such a reference frame can be visualized through a sequence of rotations and translations from the stationary frame indicated in Fig. 1.

During the unbalance whirling motion of the rotor shaft, the displacement component of point C in OZ direction is negligible. Consequently, point C is considered to move in the horizontal plane OXY. The predominant component of the angular velocity of the rotor shaft is in the OZ direction. Thus, it is convenient to visualize the displacement components of the mounting point C, with respect to a reference frame $Oxyz$ that rotates about OZ-axis at synchronous speed, as shown in Fig. 2. The displacement of point C in the plane Oxy can be defined by its coordinates (x_C, y_C). Here, the direction of Ox-axis is chosen to be that of CG, from the mounting point C to the center of mass G of the disk. The rate of change of basis vectors of the frame $Oxyz$ can be expressed as

$$\begin{bmatrix} \mathrm{d}\mathbf{i}/\mathrm{d}t \\ \mathrm{d}\mathbf{j}/\mathrm{d}t \\ \mathrm{d}\mathbf{k}/\mathrm{d}t \end{bmatrix} = \begin{bmatrix} 0 & \omega & 0 \\ -\omega & 0 & 0 \\ 0 & 0 & 0 \end{bmatrix} \begin{bmatrix} \mathbf{i} \\ \mathbf{j} \\ \mathbf{k} \end{bmatrix}. \tag{1}$$

In addition to the displacement of point C, the rotor shaft has rotation components at point C that can be visualized as three sequential Euler rotations at C. A reference frame, which is rigidly attached to the disk at point C, is more convenient to express the equations of motion. Such a

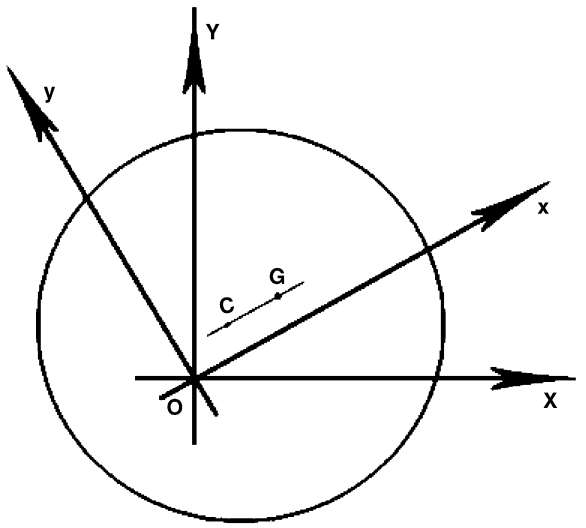

Fig. 2. Frame $Oxyz$ rotating at synchronous speed.

frame can be formed by translating frame $Oxyz$ to C and following it up by three Euler rotations. The translation of the frame $Oxyz$ to the point C results in the frame $Cx_1y_1z_1$. The first Euler rotation α about Cx_1-axis transforms $Cx_1y_1z_1$ frame to $Cx_2y_2z_2$. The second rotation β about Cy_2-axis brings $Cx_2y_2z_2$ to $Cx_3y_3z_3$. The third Euler rotation γ about Cz_3-axis completes the transformation of $Cx_3y_3z_3$ frame to $Cx'y'z'$. Last three sequential Euler rotations transform the basis vectors as

$$\begin{bmatrix} \mathbf{i}' \\ \mathbf{j}' \\ \mathbf{k}' \end{bmatrix} = \begin{bmatrix} \cos\gamma & \sin\gamma & 0 \\ -\sin\gamma & \cos\gamma & 0 \\ 0 & 0 & 1 \end{bmatrix} \begin{bmatrix} \cos\beta & 0 & -\sin\beta \\ 0 & 1 & 0 \\ \sin\beta & 0 & \cos\beta \end{bmatrix} \begin{bmatrix} 1 & 0 & 0 \\ 0 & \cos\alpha & \sin\alpha \\ 0 & -\sin\alpha & \cos\alpha \end{bmatrix} \begin{bmatrix} \mathbf{i} \\ \mathbf{j} \\ \mathbf{k} \end{bmatrix}. \tag{2}$$

The rate of change of the transformed basis vectors can be expressed as

$$\begin{bmatrix} \mathrm{d}\mathbf{i}'/\mathrm{d}t \\ \mathrm{d}\mathbf{j}'/\mathrm{d}t \\ \mathrm{d}\mathbf{k}'/\mathrm{d}t \end{bmatrix} = \begin{bmatrix} 0 & \omega_{z'} & -\omega_{y'} \\ -\omega_{z'} & 0 & \omega_{x'} \\ \omega_{y'} & -\omega_{x'} & 0 \end{bmatrix} \begin{bmatrix} \mathbf{i}' \\ \mathbf{j}' \\ \mathbf{k}' \end{bmatrix}, \tag{3}$$

where $\omega_{x'}, \omega_{y'}$ and $\omega_{z'}$ are the components of the absolute angular velocity of the disk in $Cx'y'z'$ frame. Using Eqs. (1) and (2), the expressions for these components can be obtained as

$$\omega_{x'} = \dot{\alpha}\cos\beta\cos\gamma + \dot{\beta}\sin\gamma + \omega\,(-\cos\alpha\sin\beta\cos\gamma + \sin\alpha\sin\gamma), \tag{4a}$$

$$\omega_{y'} = -\dot{\alpha}\cos\beta\sin\gamma + \dot{\beta}\cos\gamma + \omega(\sin\alpha\cos\gamma + \cos\alpha\sin\beta\sin\gamma), \tag{4b}$$

$$\omega_{z'} = \dot{\gamma} + \dot{\alpha}\sin\beta + \omega\cos\alpha\cos\beta. \tag{4c}$$

Since the variables α, β, $\dot{\alpha}$ and $\dot{\beta}$ are first-order quantities, the angular velocity component of the shaft at C in the axial direction can be approximated from Eq. (4c) as $\dot{\gamma} + \omega$. However, in the absence of torsional vibration, this axial component of the angular velocity must be equal to the speed of the shaft. Thus $\omega_{z'} = \omega$, and consequently, the variable γ must remain constant. For vector method, such a first-order approximation for the angular velocity of disk in the axial direction is acceptable. However, for scalar energy approach, the second-order error term in this angular velocity component contributes an additional term in the kinetic energy expression.

For the present vector analysis, this constant value of the variable γ can be chosen to be zero. The remaining angular velocity components can then be approximated from Eqs. (4a) and 4(b) as, $\omega_{x'} \approx (\dot{\alpha} - \beta\omega)$ and $\omega_{y'} \approx (\dot{\beta} + \alpha\omega)$.

Under first-order approximation, Eq. (2) can be simplified to $\mathbf{i} = \mathbf{i}' + \beta\mathbf{k}'$, $\mathbf{j} = \mathbf{j}' - \alpha\mathbf{k}'$ and $\mathbf{k} = -\beta\mathbf{i}' + \alpha\mathbf{j}' + \mathbf{k}'$. Consequently, the velocity and acceleration of the point C in $Cx'y'z'$ frame can be approximated as

$$\begin{aligned} \mathbf{v}_C &= v_{Cx'}\mathbf{i}' + v_{Cy'}\mathbf{j}', \\ \mathbf{a}_C &= a_{Cx'}\mathbf{i}' + a_{Cy'}\mathbf{j}', \end{aligned} \tag{5}$$

where

$$
\begin{aligned}
v_{Cx'} &= (\dot{x}_C - \omega y_C),\\
v_{Cy'} &= (\dot{y}_C + \omega x_C),\\
a_{Cx'} &= (\ddot{x}_C - 2\omega\dot{y}_C - \omega^2 x_C),\\
a_{Cy'} &= (\ddot{y}_C + 2\omega\dot{x}_C - \omega^2 y_C).
\end{aligned} \tag{6}
$$

Owing to the choice of the reference frame, the position, velocity and acceleration of the center of mass of the disk relative to C approximate to

$$
\begin{aligned}
\mathbf{r}_{G|C} &= \delta\mathbf{i}',\\
\mathbf{v}_{G|C} &= \omega\delta\mathbf{j}',\\
\mathbf{a}_{G|C} &= -\omega^2\delta\mathbf{i}'.
\end{aligned} \tag{7}
$$

The balls of the automatic balancer moves in $Cx'y'$ plane along a circular track, centered at point C. The locations of these balls in this track are defined by their angular positions ψ_i, $i = 1, 2, \ldots, n$, as shown in Fig. 3. The velocity and acceleration of the ball relative to C can be approximated to

$$
\begin{aligned}
\mathbf{v}_{B|C} &= R(\omega + \dot{\psi})(-\sin\psi\mathbf{i}' + \cos\psi\mathbf{j}') + (v_{B|C})_{z'}\mathbf{k}',\\
\mathbf{a}_{B|C} &= -R\{(\omega + \dot{\psi})^2\cos\psi + \ddot{\psi}\sin\psi\}\mathbf{i}' - R\left\{(\omega + \dot{\psi})^2\sin\psi - \ddot{\psi}\cos\psi\right\}\mathbf{j}' + (a_{B|C})_{z'}\mathbf{k}'.
\end{aligned} \tag{8}
$$

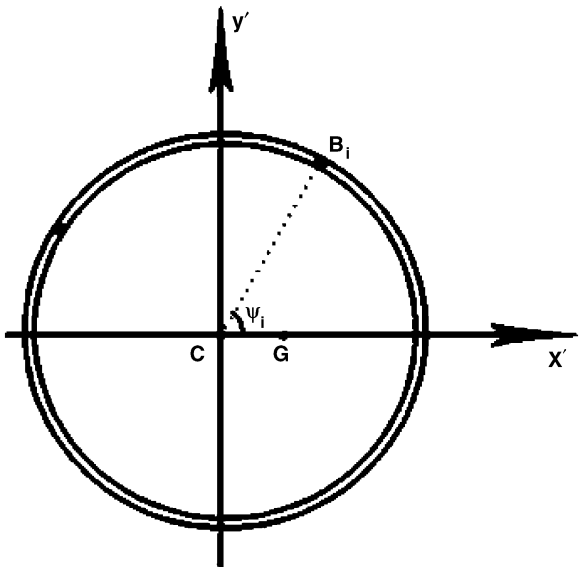

Fig. 3. Frame $Cx'y'z'$ frozen to disk.

Here, the components $(v_{B|C})_{z'}$ and $(a_{B|C})_{z'}$ in Eq. (8) are due to the rotation components of the disk about Cx' and Cy' axes. Their expressions can be obtained as

$$\begin{aligned}(v_{B|C})_{z'} &= R(\omega_{x'}\sin\psi - \omega_{y'}\cos\psi),\\ (a_{B|C})_{z'} &= R\{(\dot{\omega}_{x'} + 2\dot{\psi}\omega_{y'} + \omega\omega_{y'})\sin\psi + (-\dot{\omega}_{y'} + 2\dot{\psi}\omega_{x'} + \omega\omega_{x'})\cos\psi\}.\end{aligned}$$

2.2. Equations of motion

The inertia effects of the disk can be represented by the inertia force $\mathbf{F}_{ID}$ at G and a couple $\mathbf{M}_{ID}$. These inertia force and couple can be expressed as

$$\begin{aligned}\mathbf{F}_{ID} &= -m(a_{Cx'} - \omega^2\delta)\mathbf{i}' - ma_{Cy'}\mathbf{j}',\\ \mathbf{M}_{ID} &= -I_{x'}(\dot{\omega}_{x'} + \omega\omega_{y'})\mathbf{i}' - I_{y'}(\dot{\omega}_{y'} - \omega\omega_{x'})\mathbf{j}'.\end{aligned}$$

Under the first-order approximation, the inertia force $\mathbf{F}_{ID}$ can be moved to the point C and the resulting change in inertia couple $\mathbf{M}_{ID}$ for such movement of the inertia force is negligible. Further, the moments of inertia about axes Cx' and Cy' can be regarded as equal.

The inertia effect of the ball can be represented by the force $\mathbf{F}_{IB}$ at B. The expression for this inertia force becomes

$$\mathbf{F}_{IB} = -m_B(\mathbf{a}_C + \mathbf{a}_{B|C}).$$

The component of the moment of the force $\mathbf{F}_{IB}$ about axes Cx' and Cy' can be expressed as $-m_BR(a_{B|C})_{z'}\sin\psi$ and $m_BR(a_{B|C})_{z'}\cos\psi$, respectively. Since the mass ratio m_B/m is small, these moment components can be neglected in comparison with those of $\mathbf{M}_{ID}$.

The elastic force and moment acting on the disk at C can be expressed as

$$\begin{aligned}\mathbf{F}_{ED} &= -4k_0(x_C\mathbf{i}' + y_C\mathbf{j}') - 2k_0l(-\beta\mathbf{i}' + \alpha\mathbf{j}'),\\ \mathbf{M}_{ED} &= -2k_0l(y_C\mathbf{i}' - x_C\mathbf{j}') - \frac{4}{3}k_0l^2(\alpha\mathbf{i}' + \beta\mathbf{j}'),\end{aligned}$$

where

$$k_0 = 3EI/l^3.$$

The damping effect for translation of the disk in the surrounding air can be represented by the force $\mathbf{F}_{DT} = -c_T(\mathbf{v}_C + \mathbf{v}_{G|C})$ at G. This first-order damping force can be shifted to point C, and the error associated with such a shift is a second-order couple, which can be neglected. Similarly the moment $\mathbf{M}_{DR} = -c_R(\omega_{x'}\mathbf{i}' + \omega_{y'}\mathbf{j}')$ is introduced to represent the damping effect due to the rotation of the disk. Since the disk is assumed to be thin, the aerodynamic force associated with the rotation of this disk about Cz'-axis is not considered in the analysis. Further, the damping effect on the ball for its relative motion in the track is represented by a damping force of magnitude $c_BR\omega$ in the direction opposite to its relative motion in the frame $Cx'y'z'$.

The force and moment balance in Cx' and Cy' directions become

$$\begin{aligned}&(m + nm_B)(\ddot{x}_C - 2\omega\dot{y}_C - \omega^2x_C) + c_T(\dot{x}_C - \omega y_C) + 4k_0x_C - 2k_0l\beta\\ &\quad - \sum m_BR\{(\omega + \dot{\psi}_i)^2\cos\psi_i + \ddot{\psi}_i\sin\psi_i\} = m\omega^2\delta,\end{aligned} \tag{9}$$

$$(m+nm_B)\left(\ddot{y}_C+2\omega\dot{x}_C-\omega^2 y_C\right)+c_T\left(\dot{y}_C+\omega x_C\right)+4k_0y_C+2k_0l\alpha - \sum m_BR\{(\omega+\dot{\psi}_i)^2\sin\psi_i-\ddot{\psi}_i\cos\psi_i\}=-c_T\omega\delta, \tag{10}$$

$$I\left(\ddot{\alpha}+\omega^2\alpha\right)+c_R(\dot{\alpha}-\omega\beta)+2k_0ly_C+\tfrac{4}{3}k_0l^2\alpha=0, \tag{11}$$

$$I(\ddot{\beta}+\omega^2\beta)+c_R(\dot{\beta}+\omega\alpha)-2k_0lx_C+\tfrac{4}{3}k_0l^2\beta=0. \tag{12}$$

The equation of motion of the ith ball in the direction of its relative motion in the track can be expressed as

$$m_BR\ddot{\psi}_i+c_BR\dot{\psi}_i+m_B\left\{\left(\ddot{y}_C+2\omega\dot{x}_C-\omega^2y_C\right)\cos\psi_i-\left(\ddot{x}_C-2\omega\dot{y}_C-\omega^2x_C\right)\sin\psi_i\right\}=0. \tag{13}$$

For the investigation, the displacement and rotation components are nondimensionalized as $\bar{x}_C=x_C/\delta$, $\bar{y}_C=y_C/\delta$, $\bar{\alpha}=\alpha l/\delta$ and $\bar{\beta}=\beta l/\delta$. The variable $\bar{t}=\omega_0t$ is used to represent the nondimensional time. Here $\omega_0=\sqrt{k_0/m}$, is the characteristic bending frequency of the rotor. The other nondimensional parameters needed to rewrite Eqs. (9–13) in nondimensional form are defined as $v=m_B/m$, $\bar{I}=I/ml^2$, $\lambda=m_BR/m\delta$, $\bar{c}_T=c_T/m\omega_0$, $\bar{c}_R=c_R/I\omega_0$, $\bar{c}_B=c_B/m_B\omega_0$ and $\Omega=\omega/\omega_0$. Denoting the derivatives of the nondimensional variables with respect to the nondimensional time ω_0t by the superscript $(\,)'$, Eqs. (9–13) can be rewritten in nondimensional form as

$$(1+nv)\left(\bar{x}_C''-2\Omega\bar{y}_C'-\Omega^2\bar{x}_C\right)+\bar{c}_T\left(\bar{x}_C'-\Omega\bar{y}_C\right)+4\bar{x}_C-2\bar{\beta} - \sum\lambda\left\{\left(\Omega+\psi_i'\right)^2\cos\psi_i+\psi_i''\sin\psi_i\right\}=\Omega^2, \tag{14}$$

$$(1+nv)\left(\bar{y}_C''+2\Omega\bar{x}_C'-\Omega^2\bar{y}_C\right)+\bar{c}_T\left(\bar{y}_C'+\Omega\bar{x}_C\right)+4\bar{y}_C+2\bar{\alpha} - \sum\lambda\{(\Omega+\psi')^2\sin\psi_i-\psi_i''\cos n\psi_i\}=-\bar{c}_T\Omega, \tag{15}$$

$$\bar{I}\left(\bar{\alpha}''+\Omega^2\bar{\alpha}\right)+\bar{I}\bar{c}_R\left(\bar{\alpha}'-\Omega\bar{\beta}\right)+2\bar{y}_C+\tfrac{4}{3}\bar{\alpha}=0, \tag{16}$$

$$\bar{I}\left(\bar{\beta}''+\Omega^2\bar{\beta}\right)+\bar{I}\bar{c}_R\left(\bar{\beta}'+\Omega\bar{\alpha}\right)-2\bar{x}_C+\tfrac{4}{3}\bar{\beta}=0, \tag{17}$$

$$\lambda\psi_i''+\lambda\bar{c}_B\psi_i'+v\left\{\left(\bar{y}_C''+2\Omega\bar{x}_C'-\Omega^2\bar{y}_C\right)\cos\psi_i-\left(\bar{x}_C''-2\Omega\bar{y}_C'-\Omega^2\bar{x}_C\right)\sin\psi_i\right\}=0. \tag{18}$$

At steady state, the derivative terms in Eqs. (14–18) become zero. When $n\geqslant2$, the system of modified equations has two categories of solutions. The most useful category of balanced steady state corresponds to $\bar{x}_C=0$, $\bar{y}_C=0$, $\bar{\alpha}=0$, $\bar{\beta}=0$, $\sum\cos\psi_i=-1/\lambda$ and $\sum\sin\psi_i=\bar{c}_T/\lambda\Omega$. In addition to this balanced steady state, the system has several other unbalanced steady states, representing possible modifications of rotor whiling due to the presence of the balancing balls. However, the stability analysis of the balanced steady state is expected to provide valuable insight that will be useful in designing an effective balancing device.

For the special case $n=2$, the balancing balls have well-defined balanced steady state positions. At this stage, the analysis is continued with two balancing balls. The angular positions of the balls in the balanced steady state become $\psi_1=\psi_{10}$ and $\psi_2=\psi_{20}$ where $\cos\psi_{10}+\cos\psi_{20}=-1/\lambda$ and

$\sin\psi_{10}+\sin\psi_{20}=\bar{c}_T/\lambda\Omega$. These balanced positions of the balls can be expressed explicitly as $\psi_{10}=\pi-\psi_m-\psi_d$ and $\psi_{20}=\pi-\psi_m+\psi_d$, where $\psi_m=\arctan(\bar{c}_T/\Omega)$ and $\cos\psi_d=1/2\lambda\cos\psi_m$.

Since $\cos\psi_d\leqslant 1$, such balanced positions of the balls are possible only when $v\geq 0.5\Lambda\sqrt{(1+\bar{c}_T^2/\Omega^2)}$. Here, the parameter $\Lambda=\delta/R$ represents the residual unbalance in the rotor. Thus, the complete balancing can be realized only when the mass ratio exceeds a lower bound, which increases with the residual unbalance of the rotor. This condition for the existence of the balanced steady state can be rewritten alternatively as $\Omega\geqslant\bar{c}_T/\sqrt{(2v/\Lambda)^2-1}$ and $v\geqslant 0.5\Lambda$. Thus, the balanced steady state is possible, only when the speed exceeds a certain lower bound.

2.3. Small perturbation of equations of motion about balanced position

Considering the perturbations $\phi_1=\psi_1-\psi_{10}$ and $\phi_2=\psi_2-\psi_{20}$ to be small, the linearized equations of motion can be expressed as,

$$(1+2v)(\bar{x}_C''-2\Omega\bar{y}_C'-\Omega^2\bar{x}_C)+\bar{c}_T(\bar{x}_C'-\Omega\bar{y}_C)+4\bar{x}_C-2\bar{\beta}-\lambda\{(s_1\phi_1''+2c_1\Omega\phi_1'-s_1\Omega^2\phi_1)+(s_2\phi_2''+2c_2\Omega\phi_1'-s_2\Omega^2\phi_2)\}=0, \tag{19}$$

$$(1+2v)(\bar{y}_C''+2\Omega\bar{x}_C'-\Omega^2\bar{y}_C)+\bar{c}_T(\bar{y}_C'+\Omega\bar{x}_C)+4\bar{y}_C+2\bar{\alpha}+\lambda\{(c_1\phi_1''-2s_1\Omega\phi_1'=c_1\Omega^2\phi_1)+(c_2\phi_2''-2s_2\Omega\phi_2'-c_2\Omega^2\phi_2)\}=0, \tag{20}$$

$$\bar{I}(\bar{\alpha}''+\Omega^2\bar{\alpha})+\bar{c}_R(\bar{\alpha}'-\Omega\bar{\beta})+2\bar{y}_C+\tfrac{4}{3}\bar{\alpha}=0, \tag{21}$$

$$\bar{I}\left(\bar{\beta}''+\Omega^2\bar{\beta}\right)+\bar{c}_R\left(\bar{\beta}'+\Omega\bar{\alpha}\right)-2\bar{x}_C+\tfrac{4}{3}\bar{\beta}=0, \tag{22}$$

$$\lambda\phi_1''+\lambda\bar{c}_B\phi_1'+v\{(\bar{y}_C''+2\Omega\bar{x}_C'-\Omega^2\bar{y}_C)c_1-(\bar{x}_C''-2\Omega\bar{y}_C'-\Omega^2\bar{x}_C)s_1\}=0, \tag{23}$$

$$\lambda\phi_2''+\lambda\bar{c}_B\phi_2'+v\{(\bar{y}_C''+2\Omega\bar{x}_C'-\Omega^2\bar{y}_C)c_2-(\bar{x}_C''-2\Omega\bar{y}_C'-\Omega^2\bar{x}_C)s_2\}=0. \tag{24}$$

Here $c_1=\cos\psi_{10}$, $c_2=\cos\psi_{20}$, $s_1=\sin\psi_{10}$ and $s_2=\sin\psi_{20}$.

Substituting the modal solutions $\bar{x}_C=\tilde{x}_C\exp(s\omega_0 t)$ etc., Eqs. (19)–(24) can be expressed as a system of three matrix equations in three modal vectors $\{\tilde{x}_C\quad\tilde{y}_C\}^{\mathrm{T}}$, $\{\tilde{\alpha}\quad\tilde{\beta}\}^{\mathrm{T}}$ and $\{\tilde{\phi}_1\quad\tilde{\phi}_2\}^{\mathrm{T}}$. Eliminating the last two modal vectors, the matrix equations can be simplified to

$$\begin{bmatrix} g_1(s) & -h(s) \\ h(s) & g_2(s) \end{bmatrix}\begin{Bmatrix} \tilde{x}_C \\ \tilde{y}_C \end{Bmatrix}=\begin{Bmatrix} 0 \\ 0 \end{Bmatrix}, \tag{25}$$

where the diagonal terms $g_1(s)$ and $g_2(s)$ are sixth degree polynomials in s, while the off diagonal term $h(s)$ is a fifth degree polynomial. The characteristics equation of the linearized system becomes, $g_1g_2+h^2=0$. Routh's criteria can be used to study the stability of this system.

For the special case of the undamped linearized system, the expressions for $g_1(s)$, $g_2(s)$ and $h(s)$ can be expressed as

$$\begin{aligned}
g_1(s) &= \{s^6 + (4+\mu)s^4 + (\mu + (4-\mu)\Omega^2 - \Omega^4)s^2\} \\
&\quad + (2v)\{\Omega^2 s^4 + \mu\Omega^2 s^2 - (\mu\Omega^4 + \Omega^6)\} \\
&\quad + (v/2\lambda^2)\{s^6 + (\mu + 3\Omega^2)s^4 + (2\mu\Omega^2 + 3\Omega^4)s^2 + ((\mu\Omega^4 + \Omega^6))\}, \\
g_2(s) &= \{s^6 + (4+\mu)s^4 + (\mu + (4-\mu)\Omega^2 - \Omega^4)s^2\} \\
&\quad + (2v)\{s^6 + (\mu + 4\Omega^2)s^4 - 3(\mu\Omega^2 + \Omega^4)s^2\} \\
&\quad + (v/2\lambda^2)\{-s^6 - (\mu + 3\Omega^2)s^4 - (2\mu\Omega^2 + 3\Omega^4)s^2 - ((\mu\Omega^4 + \Omega^6))\}, \\
h(s) &= (2\Omega s)\{s^4 + (\mu + \Omega^2)s^2\} + (4v\Omega s)\{\Omega^2 s^2 + (\mu\Omega^2 + \Omega^4)\},
\end{aligned} \tag{26}$$

where, $\mu = 4/3\bar{I}$.

The characteristic equation $g_1 g_2 + h^2 = 0$ for the undamped case has terms in even powers of s only. The frequency equation of this system can be expressed as

$$g_1(jp)g_2(jp) + h^2(jp) = 0. \tag{27}$$

This twelfth degree frequency equation for the case of the undamped system has six roots for p^2, corresponding to the six vibration modes. For stability, all of these six roots for p^2 must be positive. Whenever this system is stable, the response of this undamped linear system from any arbitrary initial position must always oscillate around the balanced steady-state configuration. In the presence of damping, this linear system response must approach this balanced configuration asymptotically.

For linearization of the system, the variations in the angular positions of the balls were assumed to be small. Since this assumption is not strictly justifiable, the nonlinear equations of motion are more appropriate for the investigation of the response of the dynamical system from any arbitrary initial configuration.

3. Results and discussion

The steady-state solutions for the displacement and rotation of the unbalanced rotor alone can be obtained by setting $m_B = 0$ in Eqs. (9)–(12). In the absence of damping, the steady unbalance whirling configuration can be deduced as

$$\begin{aligned}
x_C &= -\{\Omega^2(\mu + \Omega^2)\delta\}/\{\Omega^4 - (4-\mu)\Omega^2 - \mu\}, \\
y_C &= 0, \\
\alpha &= 0, \\
l\beta &= -\{2\Omega^2\delta\}/\bar{I}\{\Omega^4 - (4-\mu)\Omega^2 - \mu\}.
\end{aligned} \tag{28}$$

Thus, the whirling amplitude will become infinite, at the speed for which $\Omega^4 - (4-\mu)\Omega^2 - \mu = 0$. The explicit expression for this critical speed can be deduced as $\Omega_c = \sqrt{\left\{\sqrt{(4-\mu+\mu^2/4)} + (2-\mu/2)\right\}}$. The expression indicates that the critical speed decreases from 2 to 1 as μ increases from zero to infinity.

An insight into this critical speed can be achieved by examining the natural vibration of the undamped rotor alone. The modal equation for this case can be simplified as

$$\begin{bmatrix} g_0(s) & -h_0(s) \\ h_0(s) & g_0(s) \end{bmatrix} \begin{Bmatrix} \tilde{x}_C \\ \tilde{y}_C \end{Bmatrix} = \begin{Bmatrix} 0 \\ 0 \end{Bmatrix}, \tag{29}$$

where $g_0(s) = \{s^4 + (4+\mu)s^2 + (\mu + (4-\mu)\Omega^2 - \Omega^4)\}$ and $h_0(s) = (2\Omega s)\{s^2 + (\mu + \Omega^2)\}$. For physical interpretation, the frequency equation of this undamped rotor in the synchronous rotating frame can be factorized into the forward and backward frequency equations [2]. From Eq. (29), the forward frequency equation of the undamped rotor can be expressed as $g_0(jp) + jh_0(jp) = 0$. Using the expressions for $g_0(s)$ and $h_0(s)$, this forward frequency equation can be simplified to

$$\left\{p_0^4 + 2\Omega p_0^3 - (4+\mu)p_0^2 - 2\Omega\left(\mu + \Omega^2\right)p_0 + \left(\mu + (4-\mu)\Omega^2 - \Omega^4\right)\right\} = 0. \tag{30}$$

Comparison of Eqs. (28) and (30) indicates that the whirling amplitude becomes infinite at the speed for which the natural frequency of the rotor in the synchronous rotating frame vanishes. The variations of the four natural frequencies of the rotor with speed for the case $\bar{I} = 0.25$ are shown in Fig. 4 as continuous lines. The frequencies $q_0 = p_0 + \Omega$ in a stationary frame are indicated by the dashed lines [2]. Thus, the critical speed of the rotor coincides with the forward synchronous natural frequency of the rotor in a stationary reference frame. Information on the effectiveness of the automatic balancer around this critical speed is very useful in suppressing the whirling amplitude of the rotor.

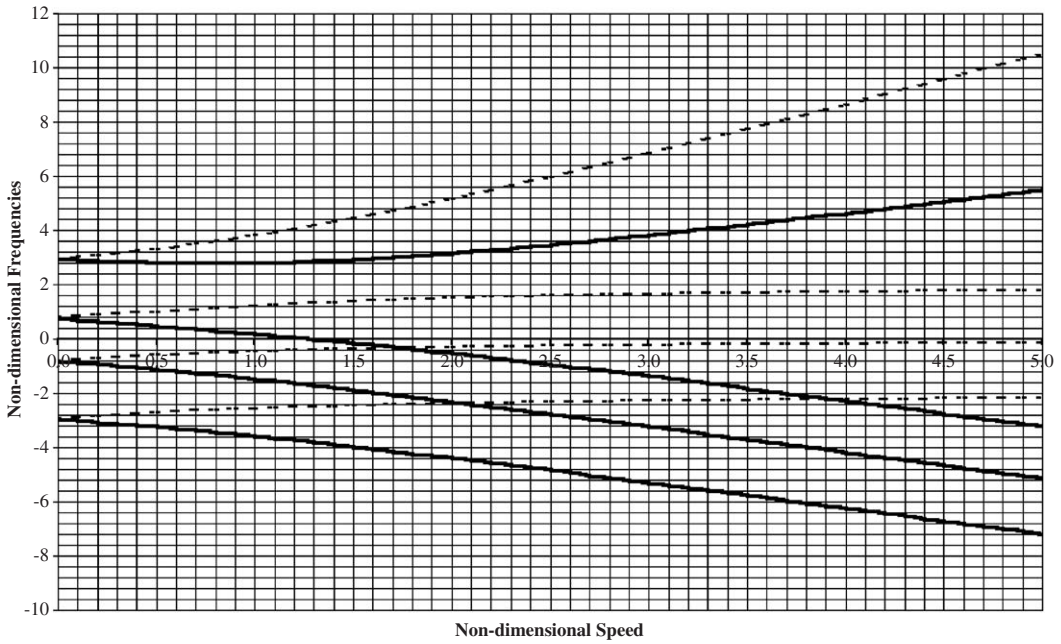

Fig. 4. Variation of rotor frequencies with speed, $\bar{I} = 0.25$: ————, rotating frame; – – – –, stationary frame.

The presence of the balancing balls modifies the rotor frequencies and introduces two additional frequencies. Furthermore, the balanced steady state of this system is stable only when the natural frequencies of all six natural modes are real. The roots of the frequency Eq. (27) of the undamped system depends on the nondimensional speed Ω and the system parameters $\bar{I}$, v and λ. For physical interpretation, it is desirable to replace the parameter λ with $\Lambda = (v/\lambda) = (\delta/R)$, which represents the residual unbalance in the rotor.

Having chosen $\bar{I} = 0.25$ and $\Lambda = 0.05$, the mass ratio v was varied from 0.01 to 0.10 in steps of 0.01, and the corresponding speed ranges within which the frequency equation (27) has six positive roots for p^2 were identified. For this purpose, the speed Ω was first varied from 0.1 to 5.00 in steps of 0.1, and the particular steps within which the stability boundary speed lies were identified. The stability boundary speeds were then calculated to five decimal place accuracy. The variation of the stable speed range with mass ratio for the case $\bar{I} = 0.25$ and $\Lambda = 0.05$ is shown in Fig. 5. Repeated computations using various combinations of the system parameters $\bar{I}$, v and Λ indicate that the linear undamped system remains stable within one or more intervals of speed.

For the case $\bar{I} = 0.25$, $v = 0.05$ and $\Lambda = 0.05$, the variation of the undamped system frequencies with speed is shown in Fig. 6. This result indicates that the number of stable modes of the linearized system at the nondimensional speeds $\Omega = 1.0$, $\Omega = 2.5$, $\Omega = 3.5$ and $\Omega = 4.5$ as 4, 2, 6 and 2, respectively. When the nondimensional speed Ω lies between 3.1907 and 3.7059, all six natural modes of the system have real natural frequencies and consequently, the balanced steady state is stable within this speed range.

When the undamped linear system is stable, its response from any initial conditions is known to be a mixed mode oscillation about its steady-state configuration. Further, the presence of

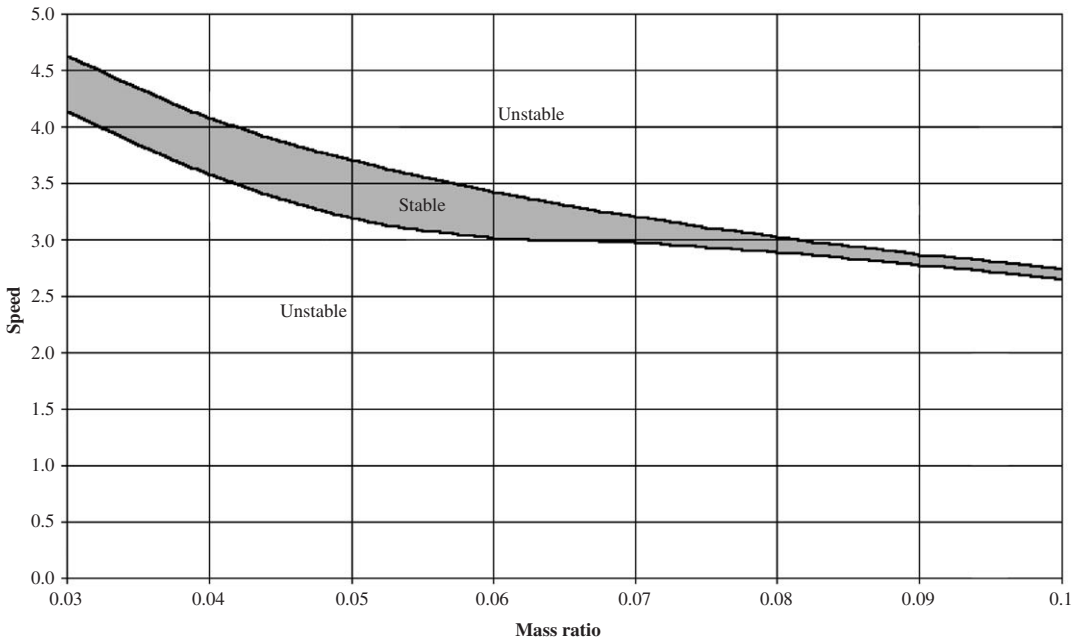

Fig. 5. Variation of stable speed range with mass ratio, $\bar{I} = 0.25$, $\Lambda = 0.05$.

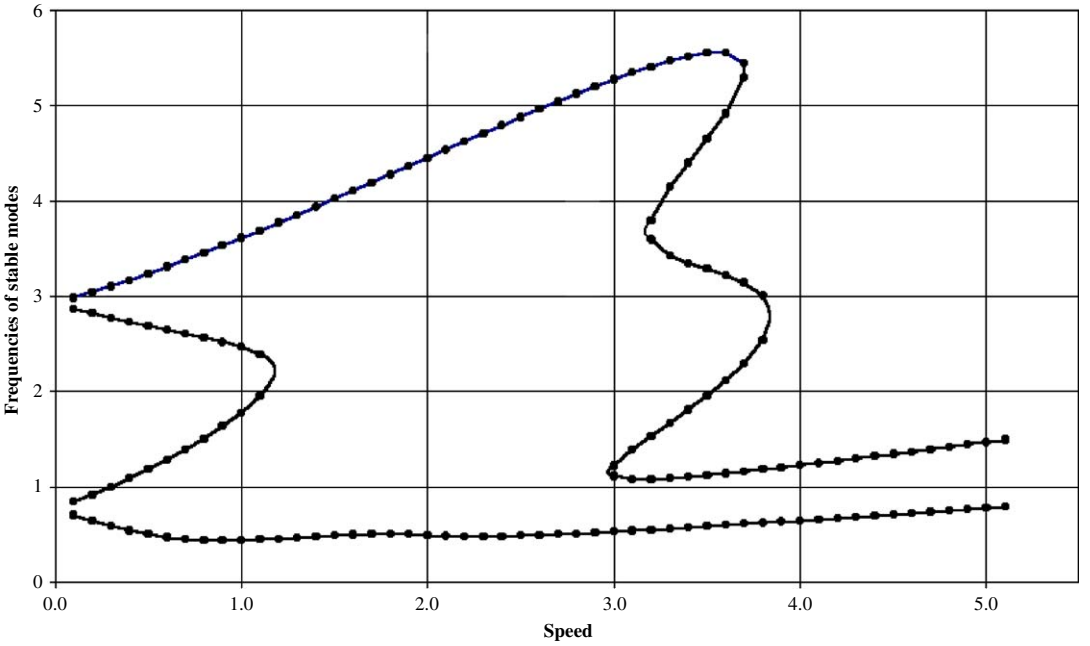

Fig. 6. Variation of frequencies of stable modes with speed, $\bar{I} = 0.25$, $\nu = 0.05$, $\Lambda = 0.05$.

damping in a stable linear system dissipates the vibrational energy and enables the response to approach this steady-state position asymptotically. Thus, the computation of the response of the linearized system at a stable speed can be used to evaluate the accuracy and suitability of the numerical methods for such response studies.

Fourth-order Adams–Moulton predictor–corrector method is used iteratively to compute the response. The response values for the first four starting steps were obtained using a sixth-order Runge–Kutta method with known error estimate. The initial step size in the Runge–Kutta algorithm is controlled to keep the local accuracy to the fifth order. A trial application of this algorithm to the damped linearized system justifies its suitability to study the response of the nonlinear system.

Owing to the unrestrained motion of the balancing balls in their track, the linearizing assumptions that the variations $\phi_1 = \psi_1 - \psi_{10}$ and $\phi_2 = \psi_2 - \psi_{20}$ of balancing ball angular positions are small are not justifiable. Further, when ψ_1' and ψ_2' are not small, the linearization of the centrifugal force term in the equations of motion could possibly introduce additional errors. Thus, it becomes necessary to study the system response using the nonlinear governing equations. The system parameters for the non linear system response study are chosen as $\bar{I} = 0.25$, $\nu = 0.05$, $\Lambda = 0.05$, $\bar{c}_T = 2.0$, $\bar{c}_R = 1.0$ and $\bar{c}_B = 1.0$. The initial conditions, $\bar{x}_C = \bar{y}_C = 0$, $\bar{x}_C' = \bar{y}_C' = 0$, $\bar{\alpha} = \bar{\beta} = 0$, $\bar{\alpha}' = \bar{\beta}' = 0$, $\psi_1 = 0$, $\psi_2 = \pi$, $\psi_1' = \psi_2' = 0$ are used for the nonlinear response analysis.

At $\Omega = 3.5$, Fig. 6 indicates that the linearized undamped system is stable. The results of the nonlinear response analysis indicate the variations of the displacement components $\bar{x}_C$ and $\bar{y}_C$ with time $\omega_0 t$ at speed $\Omega = 3.5$ as shown in Fig. 7. The corresponding variations of the rotation

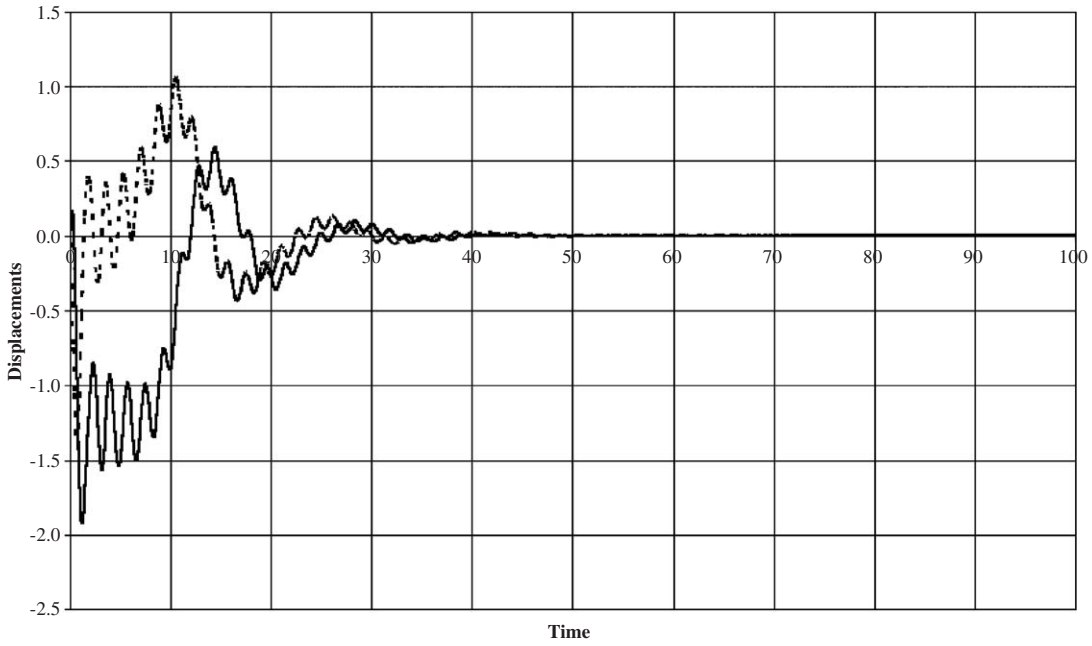

Fig. 7. Variation of displacement components with time, $\bar{I} = 0.25$, $v = 0.05$, $\Lambda = 0.05$, $\Omega = 3.5$: ————, $\bar{x}_C$; ------, $\bar{y}_C$.

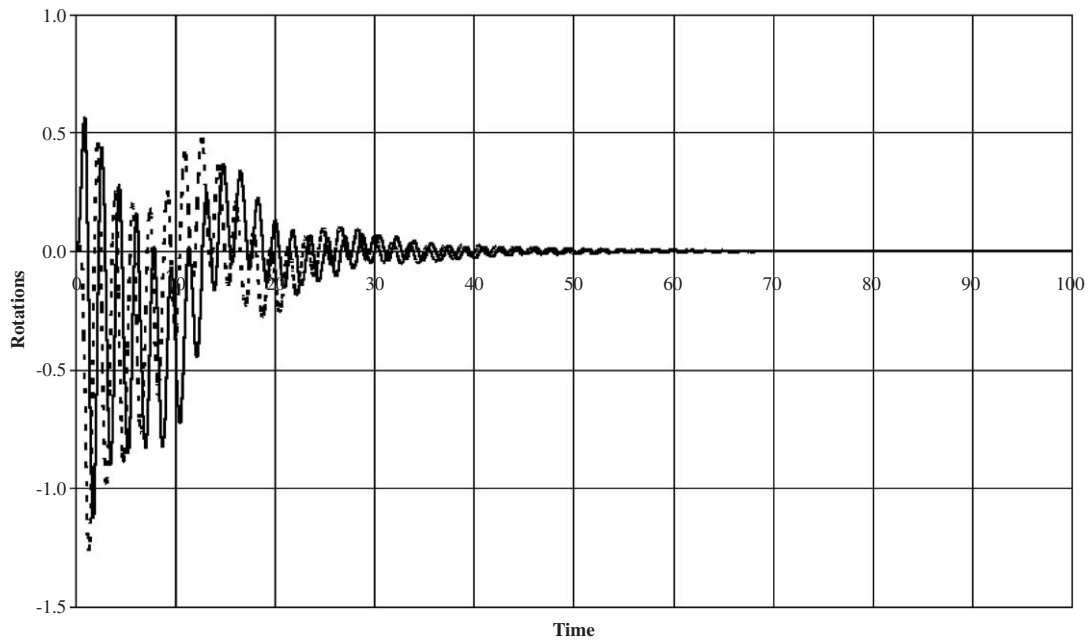

Fig. 8. Variation of rotation components with time, $\bar{I} = 0.25$, $v = 0.05$, $\Lambda = 0.05$, $\Omega = 3.5$: ————, $\bar{\alpha}$; ------, $\bar{\beta}$.

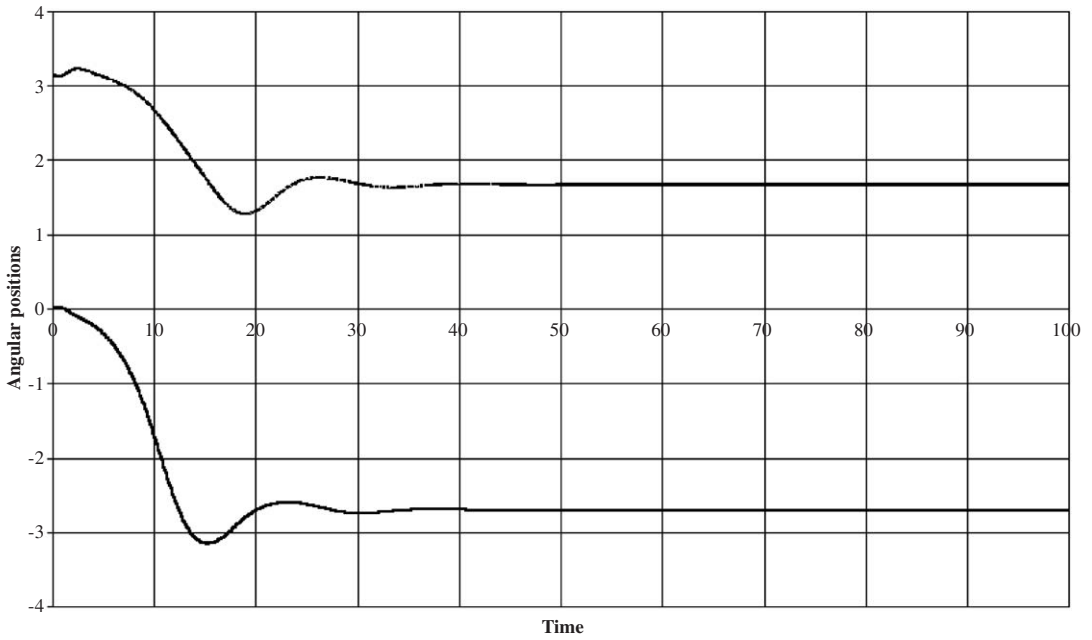

Fig. 9. Variation of angular positions of balls with time, $\bar{I} = 0.25$, $v = 0.05$, $\Lambda = 0.05$, $\Omega = 3.5$: ————, ψ_1; ------, ψ_2.

components $\bar{\alpha}$ and $\bar{\beta}$, and the angular positions ψ_1 and ψ_2 of the balancing balls are shown in Figs. 8 and 9, respectively. At $\Omega = 3.5$, the steady-state angular positions of the balancing balls can be calculated as $\psi_{10} = 1.6653$ and $\psi_{20} = 2\pi - 2.7036$. The response clearly converges to the balanced steady-state configuration of the system.

There is a possibility of collisions of the balls within the track during this response period. Since the velocities of the masses are exchanged during perfectly elastic collisions of equal masses, the consequence of such collisions can be ignored in the response computation.

The system has unbalanced steady states also. The influence of the initial conditions on the system response is investigated by changing the initial ball positions to $\psi_1 = \psi_2 = 0$, while maintaining the other initial conditions at their earlier values. The response of the system under the modified initial conditions is shown in Figs. 10–12. In these variations, the balls move together in complete circles and the system response does not approach a definite steady state. Further, the nature of this limit response can be understood from the plot of $\bar{y}_C$ against $\bar{x}_C$, shown in Fig. 13. In this case, the limit response of the system can be identified as a limiting cyclic motion around an unbalanced steady state. Thus, the initial positions of the balls have significant influence on the ultimate steady state of the system. Further, it demonstrates the limitations of the linearized analysis of the system.

The former initial conditions $\psi_1 = 0$ and $\psi_2 = \pi$ are restored for further response studies at $\Omega = 4.5$, $\Omega = 2.5$ and $\Omega = 1.0$. Linearized undamped analysis indicated that the balanced steady state of the system at these three speeds is unstable. However, Figs. 14–19 reveal that the system responses at $\Omega = 4.5$ and $\Omega = 2.5$ for the chosen initial conditions are stable and ultimately

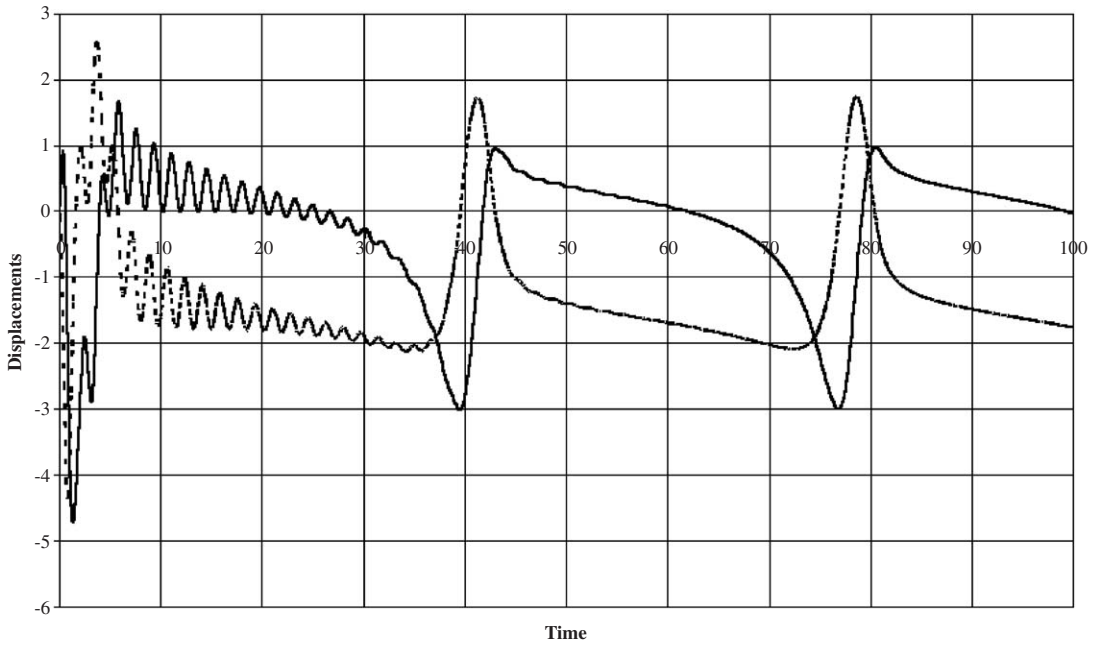

Fig. 10. Variation of displacement components with time, $\bar{I} = 0.25$, $v = 0.05$, $\Lambda = 0.05$, $\Omega = 3.5$ (modified initial conditions): ————, $\bar{x}_C$; ------, $\bar{y}_C$.

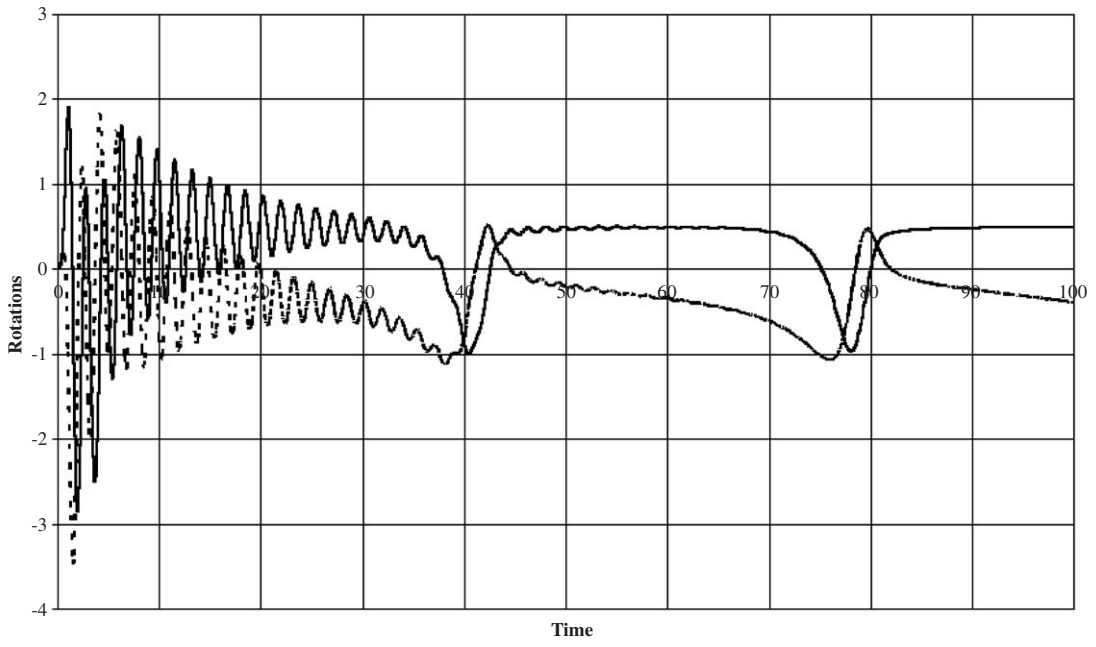

Fig. 11. Variation of rotation components with time, $\bar{I} = 0.25$, $v = 0.05$, $\Lambda = 0.05$, $\Omega = 3.5$ (modified initial conditions): ————, $\bar{\alpha}$; ------, $\bar{\beta}$.

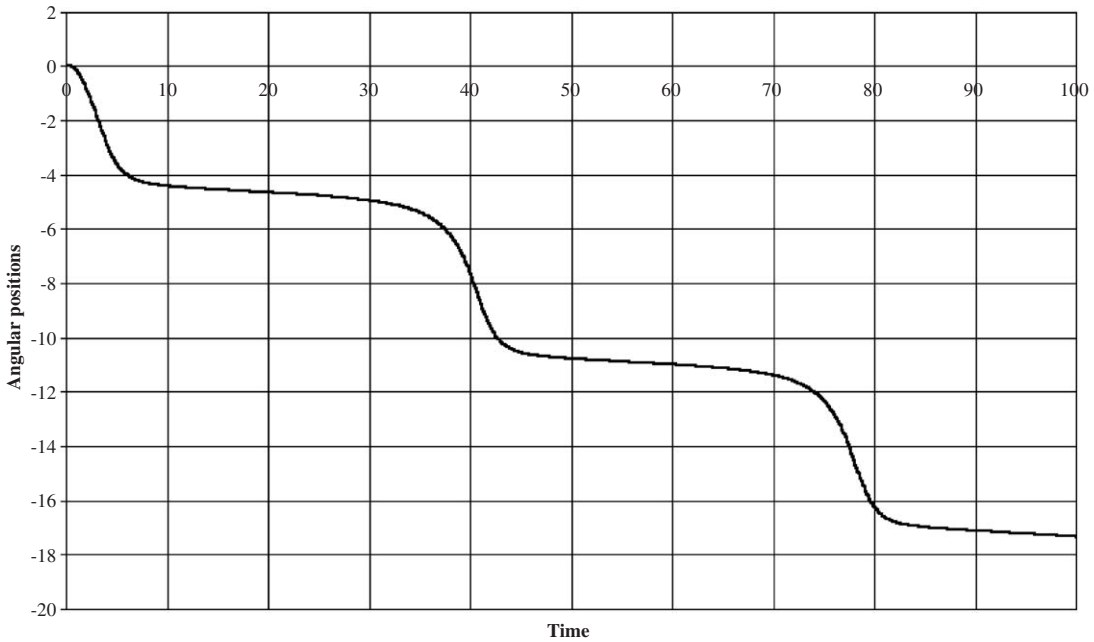

Fig. 12. Variation of angular positions of balls with time, $\bar{I} = 0.25$, $v = 0.05$, $\Lambda = 0.05$, $\Omega = 3.5$ (modified initial conditions): ————, ψ_1; ------, ψ_2.

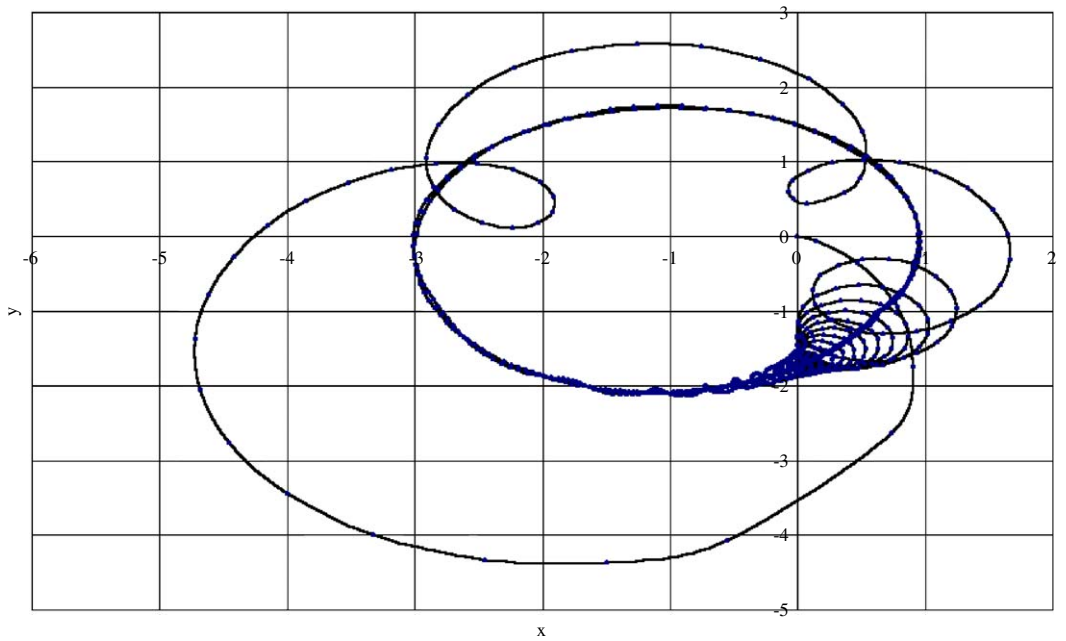

Fig. 13. Locus of mounting point, $\bar{I} = 0.25$, $v = 0.05$, $\Lambda = 0.05$, $\Omega = 3.5$ (modified initial conditions).

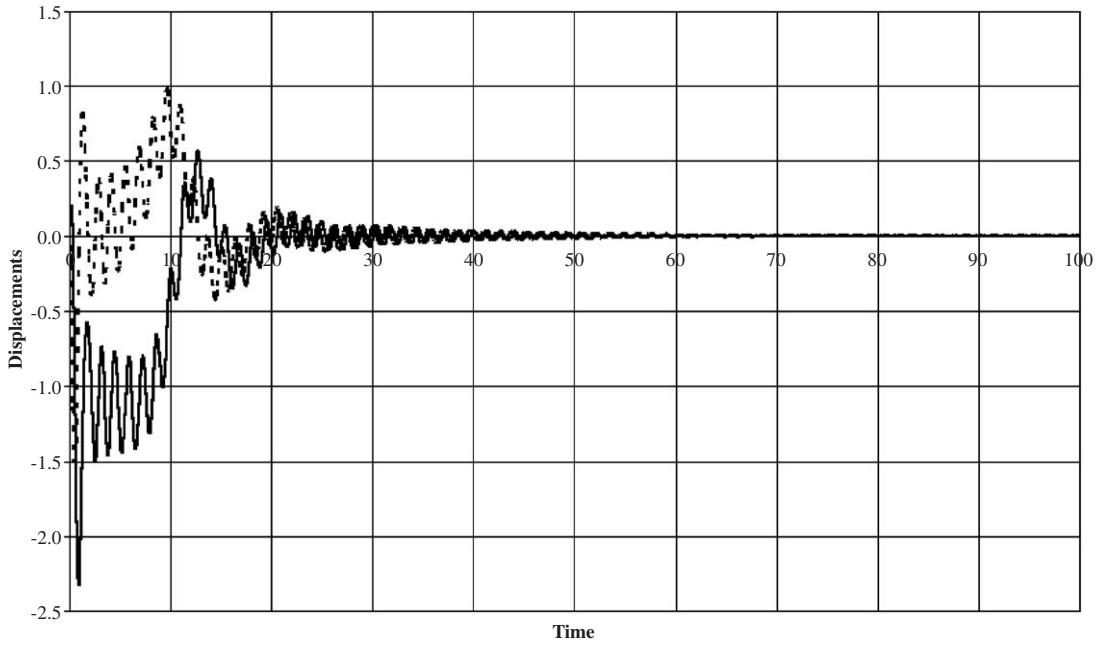

Fig. 14. Variation of displacement components with time, $\bar{I} = 0.25$, $v = 0.05$, $\Lambda = 0.05$, $\Omega = 4.5$: ————, $\bar{x}_C$; ------, $\bar{y}_C$.

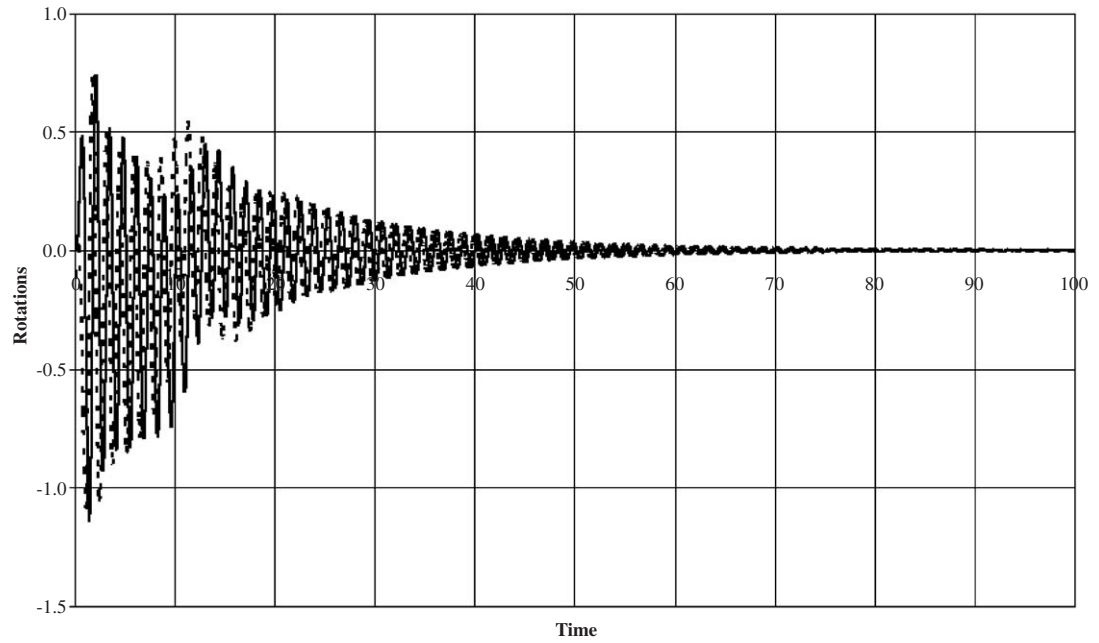

Fig. 15. Variation of rotation components with time, $\bar{I} = 0.25$, $v = 0.05$, $\Lambda = 0.05$, $\Omega = 4.5$: ————, $\bar{\alpha}$; ------, $\bar{\beta}$.

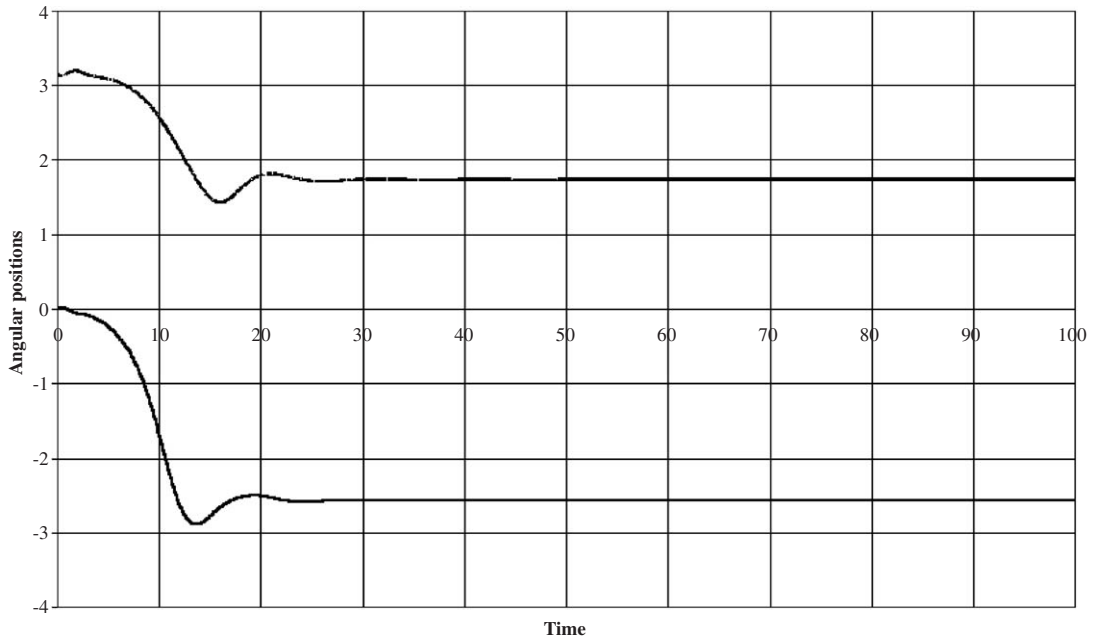

Fig. 16. Variation of angular positions of balls with time, $\bar{I} = 0.25$, $v = 0.05$, $\Lambda = 0.05$, $\Omega = 4.5$: ————, ψ_1; ------, ψ_2.

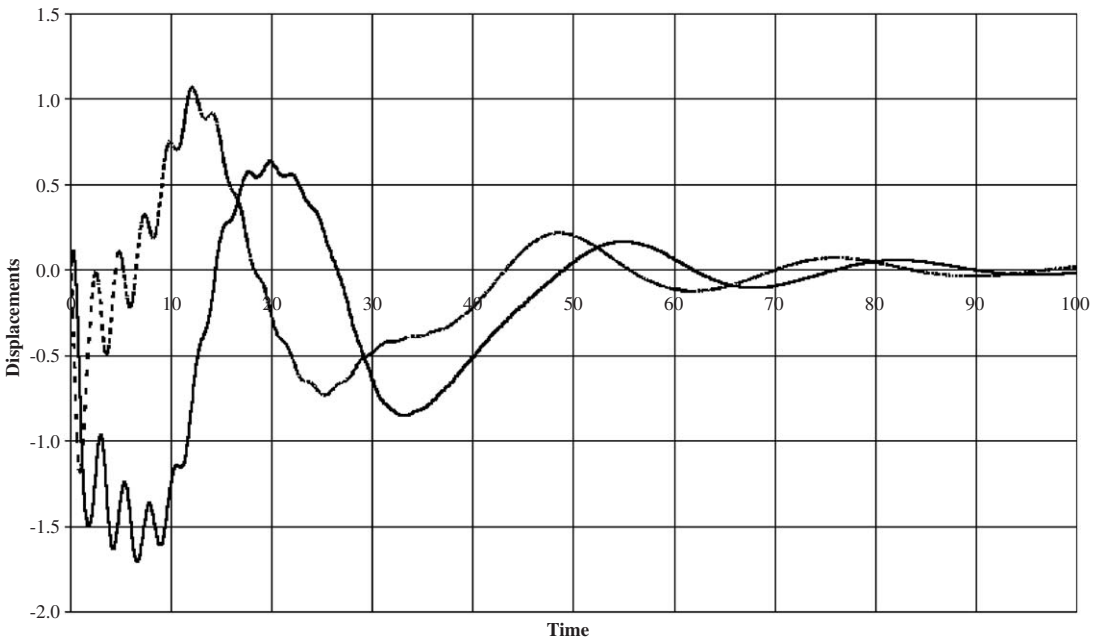

Fig. 17. Variation of displacement components with time, $\bar{I} = 0.25$, $v = 0.05$, $\Lambda = 0.05$, $\Omega = 2.5$: ————, $\bar{x}_C$; ------, $\bar{y}_C$.

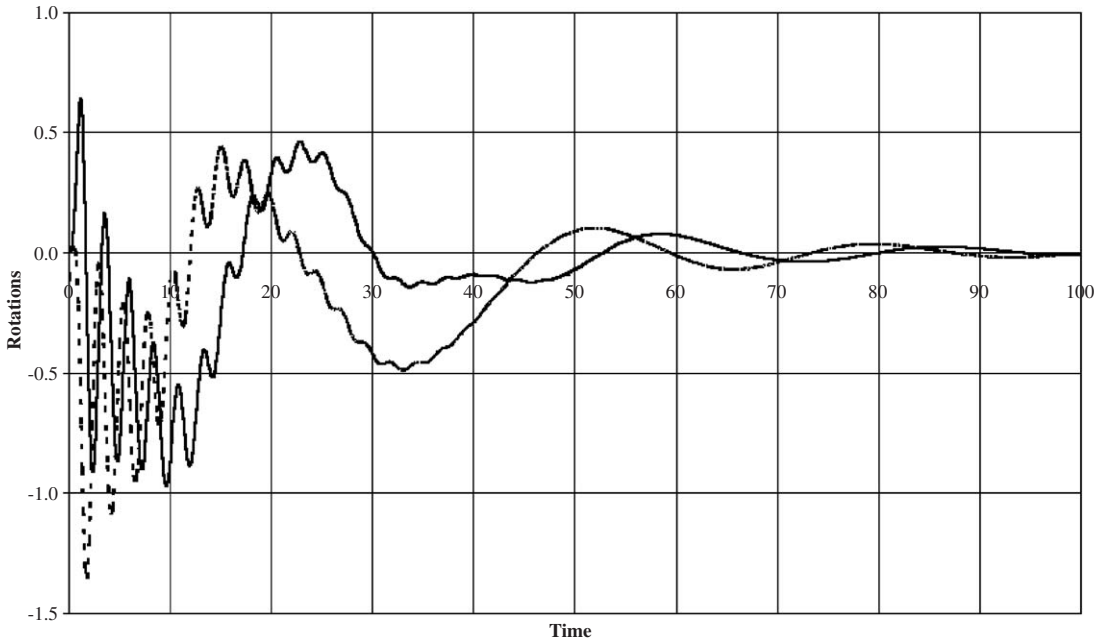

Fig. 18. Variation of rotation components with time, $\bar{I} = 0.25$, $v = 0.05$, $\Lambda = 0.05$, $\Omega = 2.5$: ————, $\bar{\alpha}$; ------, $\bar{\beta}$.

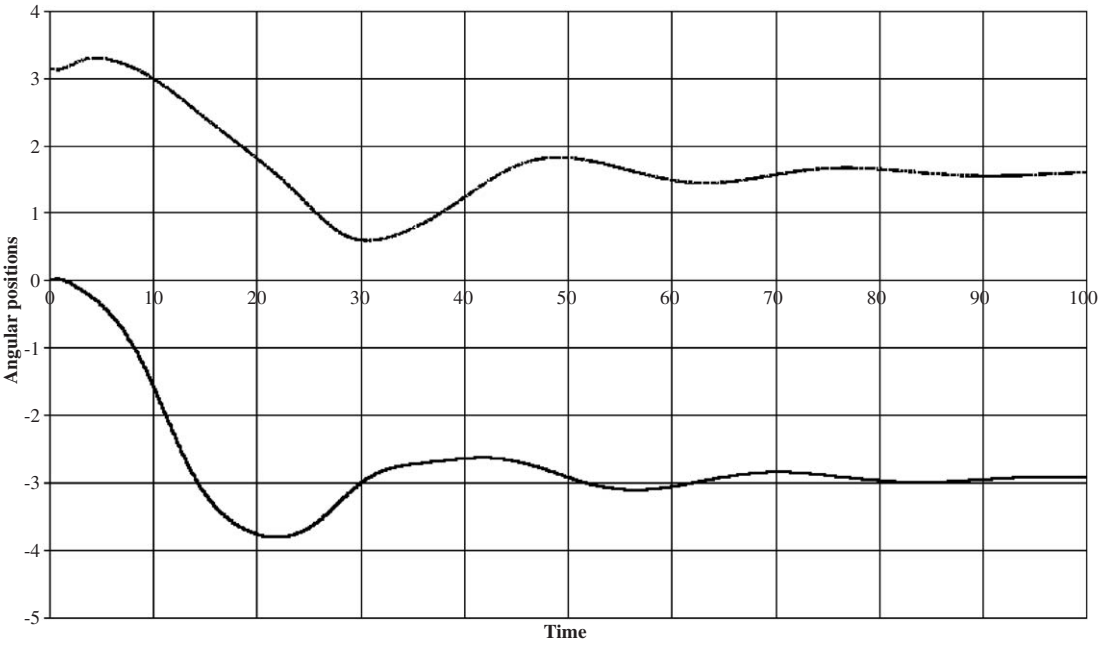

Fig. 19. Variation of angular positions of balls with time, $\bar{I} = 0.25$, $v = 0.05$, $\Lambda = 0.05$, $\Omega = 2.5$: ————, ψ_1; ------, ψ_2.

approach the balanced steady state. Thus, the linearized undamped analysis is not accurate enough to predict the stability of the balanced steady state. As mentioned earlier, the linearizing assumption that the variations of ψ_1 and ψ_2 remain small is not justifiable. The cyclic nature of the variables $\psi_1$and ψ_2, and the strong nonlinearity in the centrifugal force term in the equations of motion suggests the necessity of nonlinear analysis for this system.

Because of the presence of damping in the system, the balanced steady state is realizable only for higher speeds in the range $\Omega \geqslant 1.1547$. Thus, at $\Omega = 1.0$, the system does not have a balanced steady state. Figs. 20–22 indicates the response of the system at $\Omega = 1.0$. In this case, the balancing balls move towards the same angular position $\psi_1 = \psi_2$, which corresponds to an unbalanced steady state of the system (Fig. 20) [4].

In the present response analysis, a set of 12 initial conditions are used in addition to the seven nondimensional parameters that identify the system. Owing to the possibility of large number data sets, the system cannot be analyzed completely. For certain data sets, the response stabilizes to either a balanced or an unbalanced steady state. In certain other cases, the response is found to approach a limit cycle.

The scope of the present investigation is restricted to the analysis of the system response at constant operating speed. The balancing device that suppresses whirling motion of the rotor for all possible initial conditions is considered to be effective. This investigation is a step in identifying the factors that enhance the effectiveness of the balancing device. Analysis using a simplified system model must be attempted first to identify the factors that can enhance the effectiveness of the automatic balancing device.

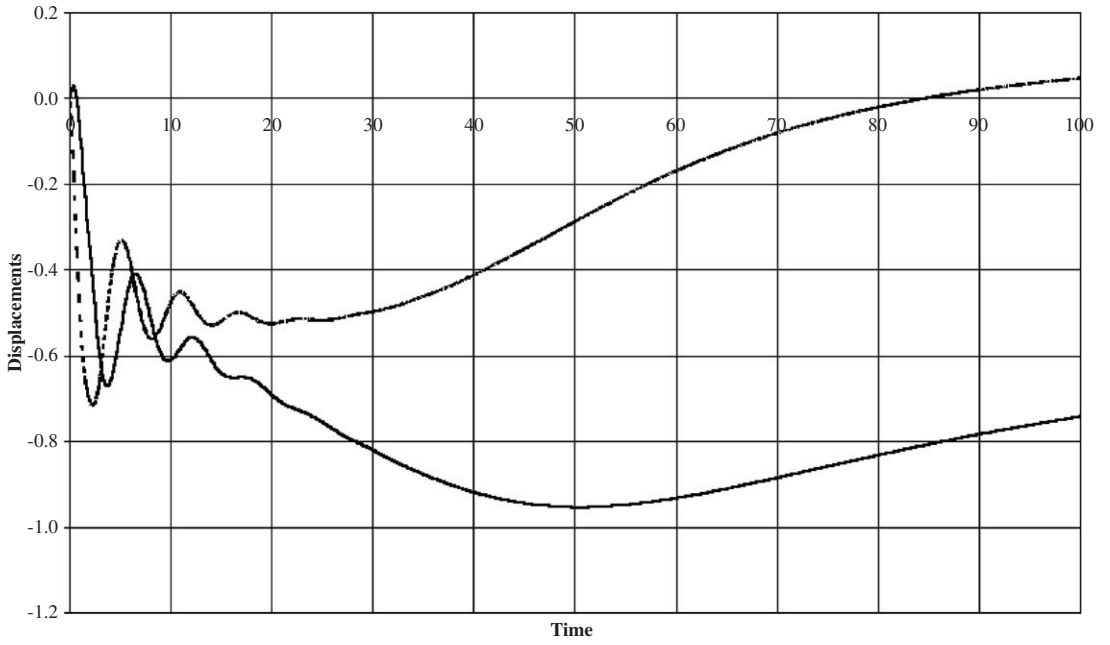

Fig. 20. Variation of displacement components with time, $\tilde{I} = 0.25$, $v = 0.05$, $\Lambda = 0.05$, $\Omega = 1.0$: ————, $\bar{x}_C$; ------, $\bar{y}_C$.

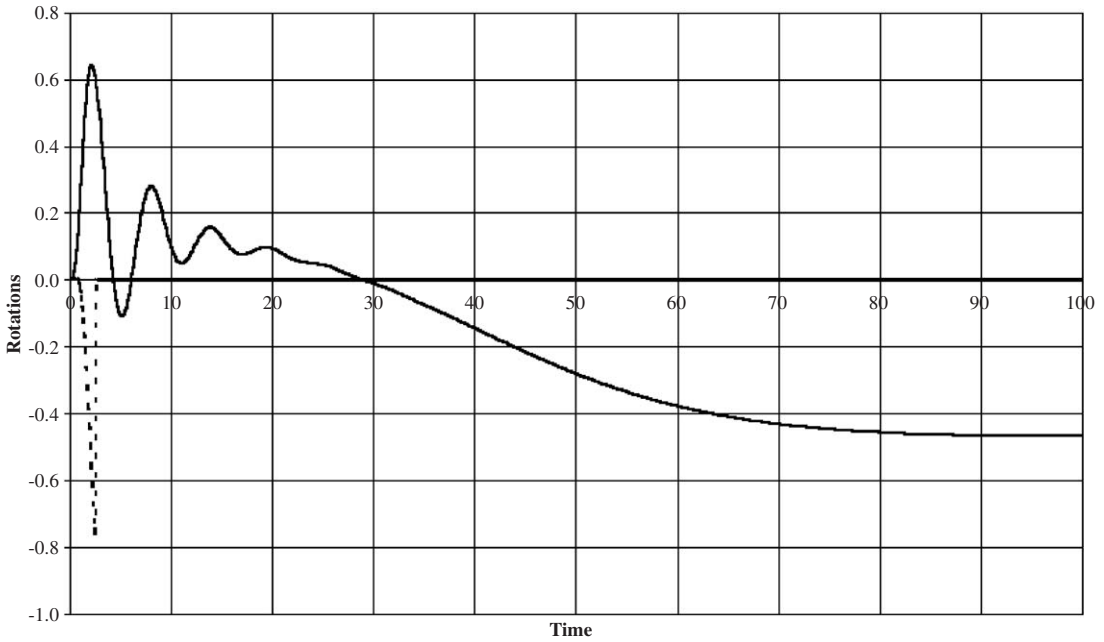

Fig. 21. Variation of rotation components with time, $\bar{I} = 0.25$, $v = 0.05$, $\Lambda = 0.05$, $\Omega = 1.0$: ————, $\bar{\alpha}$; ------, $\bar{\beta}$.

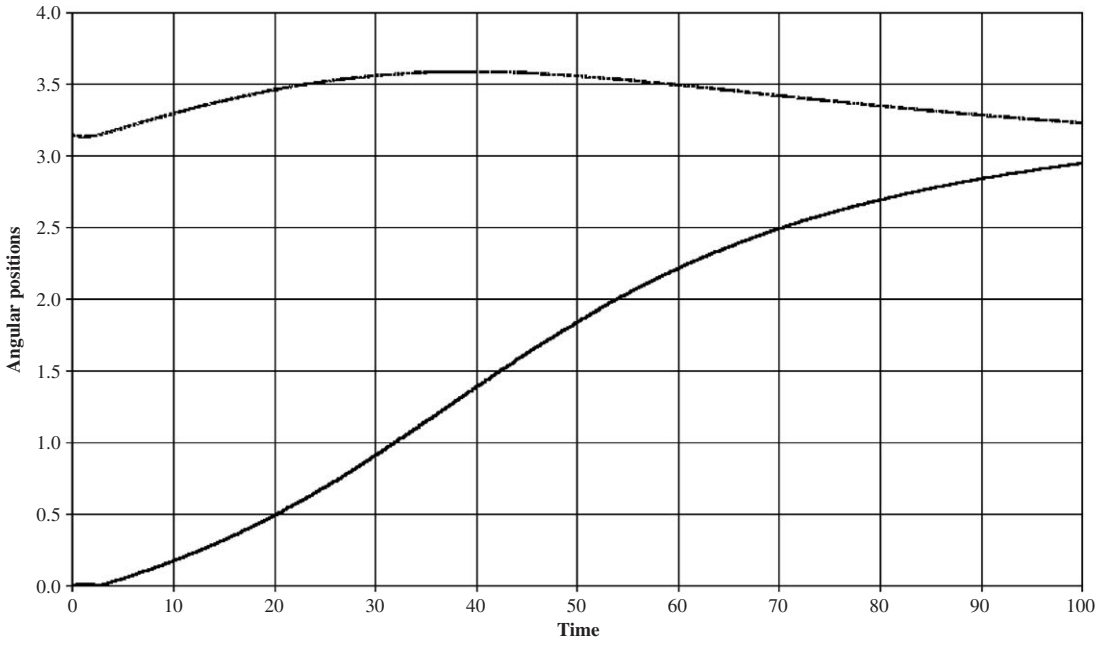

Fig. 22. Variation of angular positions of balls with time, $\bar{I} = 0.25$, $v = 0.05$, $\Lambda = 0.05$, $\Omega = 1.0$: ————, ψ_1; ------, ψ_2.

4. Conclusions

The suitability of automatic balancing devise to completely balance the residual imbalance in a disk mounted on a flexible cantilever shaft is investigated. The translation and the rotation of the disk during unbalanced whirling motion and the consequent damping influence are considered in the analysis. Seven nondimensional parameters are used to define this damped system.

Two balancing balls are used to realize the balanced steady-state configuration of the system. A minimum mass of the balancing ball is required to realize this balanced steady state. Besides the balanced steady state, the system has several unbalanced steady states.

Linearized vibration analysis of the system about its balanced steady-state configuration is used to determine the stable speed range of this state. The more accurate nonlinear response analysis showed that the linearized stability analysis is not always accurate. In certain cases, the nonlinear response is found to depend strongly on the chosen initial conditions.

The nonlinear response analysis of the system indicates that the system either stabilizes to a steady-state configuration or settles down to a limit-cycle vibration. In certain cases, the initial conditions play a decisive role in the determination of the ultimate state of the system response. However, the investigation revealed that, under certain conditions, the system stabilizes to its balanced steady state and thereby balances the residual imbalance completely.

Because of the complexity of the system model, the analysis could not pin point directly the factors that can enhance the effectiveness of the automatic balancing device. Analysis using a simplified system model is more appropriate to eke out results that are more useful to the design of an effective balancer.

References

[1] J.P. Den Hartog, *Mechanical Vibrations*, Dover, New York, 1985.
[2] A. Tondl, *Some Problems in Rotordynamics*, Chapman & Hall, London, 1965.
[3] H. Lindell, Vibration reduction on hand-held grinders by automatic balancers, *Central European Journal of Public Health* 4 (1996) 43–45.
[4] C. Rajalingham, R.B. Bhat, S. Rakheja, Automatic balancing of flexible vertical rotors using a guided ball, *International Journal of Mechanical Sciences* 9 (1998) 825–834.
[5] C. Rajalingham, S. Rakheja, Whirl suppression in hand-held power tool rotors using guided rolling balancers, *Journal of Sound and Vibration* 217 (1998) 453–466.
[6] C.H. Hwang, J. Chung, Dynamic analysis of an automatic ball balancer with double races, *JSME International Journal* 42 (1999) 265–272.
[7] J. Chung, I. Jang, Dynamic response and stability analysis of an automatic ball balancer for a flexible rotor, *Journal of Sound and Vibration* 259 (2003) 31–43.